Journal of Coordination Chemistry

ISSN: 0095-8972 (Print) 1029-0389 (Online) Journal homepage: http://www.tandfonline.com/loi/gcoo20

The assembly of POM-induced inorganic–organic hybrids based on copper ions and mixed ligands

Dan-Dan Yang, Bao Mu, Lei Lv & Ru-Dan Huang

To cite this article: Dan-Dan Yang, Bao Mu, Lei Lv & Ru-Dan Huang (2015) The assembly of POM-induced inorganic–organic hybrids based on copper ions and mixed ligands, Journal of Coordination Chemistry, 68:5, 752-765, DOI: 10.1080/00958972.2015.1009906

To link to this article: http://dx.doi.org/10.1080/00958972.2015.1009906

Journal of Coordination Chemistry, 2015
Vol. 68, No. 5, 752–765, http://dx.doi.org/10.1080/00958972.2015.1009906

The assembly of POM-induced inorganic–organic hybrids based on copper ions and mixed ligands

DAN-DAN YANG, BAO MU, LEI LV and RU-DAN HUANG*

Key Laboratory of Cluster Science of Ministry of Education, School of Chemistry, Beijing Institute of Technology, Beijing, PR China

(*Received 14 August 2014; accepted 8 January 2015*)

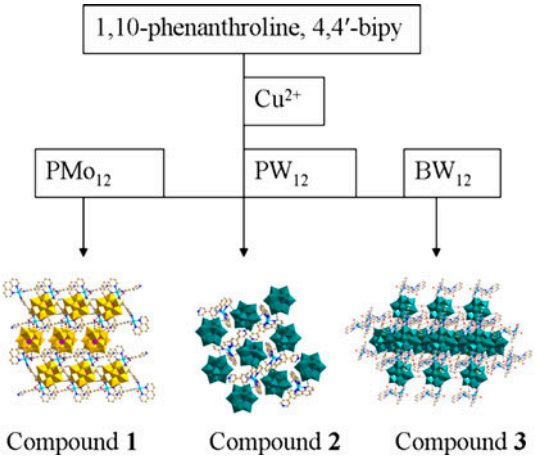

Though PMo_{12}, PW_{12}, and BW_{12} are all Keggin-type POMs, they exhibit different coordination abilities and electron densities under different pH conditions. Therefore, the types of POMs and pH value have effects on the formation of various frameworks.

Three inorganic–organic hybrid materials based on Keggin-type polyoxometalates (POMs), $[Cu^{II}_2(phen)_2(4,4'\text{-bipy})(H4,4'\text{-bipy})_2(H_2O)_2][PMo_{12}O_{40}]_2\cdot 2H_2O$ (**1**), $[Cu^{II}(phen)_2(H4,4'bipy)][PW_{12}O_{40}]\cdot H_2O$ (**2**), and $[Cu^{II}_2(phen)_2(4,4'\text{-bipy})(BW_{12}O_{40})(H_2O)_2](H_24,4'\text{-bipy})_{0.5}\cdot 3H_2O$ (**3**) (phen = 1,10-phenanthroline, 4,4′-bipy = 4,4′-bipyridine), were synthesized using different POMs in the hydrothermal conditions. Compounds **1–3** were characterized by single-crystal X-ray diffraction, IR spectra, elemental analyses, powder X-ray diffraction analyses, and thermogravimetric analyses. Compound **1** presents a two-dimensional (2-D) network containing the Keggin-type $[PMo_{12}O_{40}]^{3-}$ anion and dinuclear metal–organic units $[Cu^{II}_2(phen)_2(4,4'\text{-bipy})(H4,4'\text{-bipy})_2(H_2O)_2]^{3+}$. Compound **2** is a 2-D architecture constructed from a $[PW_{12}O_{40}]^{3-}$ and mononuclear metal–organic units $[Cu^{II}(phen)_2(H4,4'\text{-bipy})]^{3+}$. In **3**, the $[BW_{12}O_{40}]^{5-}$ anions link $[Cu^{II}_2(phen)_2(4,4'\text{-bipy})]$ units to form a one-dimensional (1-D) chain $[Cu^{II}_2(phen)_2(4,4'\text{-bipy})(BW_{12}O_{40})(H_2O)_2]$; the 1-D chain connects with protonated 4,4′-bipy ligands and lattice waters, yielding a 2-D layer. Fluorescence spectra, UV–vis spectra, and electrochemical properties of **1–3** have been investigated.

*Corresponding author. Email: huangrd@bit.edu.cn

Keywords: Inorganic–organic hybrid materials; Keggin-type polyoxometalates; Copper ions; 2-D structure; Electrochemical property

1. Introduction

Polyoxometalates (POMs) are anionic metal oxide clusters of early transition metals, such as molybdenum, vanadium, and tungsten. Because of special structural features and properties, they have been applied in catalysis, magnetism, porous materials, medicine, biology, photochemistry [1–6], etc. The design and synthesis of POM-based inorganic–organic hybrid materials have attracted interest due to their diverse structures and potential applications, such as electrocatalysis, selective absorption of gas [7–9], etc. Keggin-type POMs are important inorganic ligands to build POM-based inorganic–organic hybrid compounds because of saturated structure and large electron density [10, 11].

Phen [12] and 4,4′-bipy (phen = 1,10-phenanthroline, 4,4′-bipy = 4,4′-bipyridine) are N-donor ligands. Many hybrids based on POMs and phen or 4,4′-bipy have been reported [13, 14]. However, only a few examples combine both phen and 4,4′-bipy with POMs [15, 16, 36]. Compared with previously reported compounds, **1–3** contain the same ligands and copper ions and diverse Keggin POMs; however, they exhibit different constructions. In this work, three different organic–inorganic hybrids based on POMs, $[Cu^{II}_2(phen)_2(4,4'\text{-bipy})(H4,4'\text{-bipy})_2(H_2O)_2][PMo_{12}O_{40}]_2\cdot 2H_2O$ (**1**), $[Cu^{II}(phen)_2(H4,4'bipy)][PW_{12}O_{40}]\cdot H_2O$ (**2**), and $[Cu^{II}_2(phen)_2(4,4'\text{-bipy})(BW_{12}O_{40})(H_2O)_2](H_24,4'\text{-bipy})_{0.5}\cdot 3H_2O$ (**3**), are obtained. Compounds **1–3** are all two-dimensional (2-D) supramolecular networks with different frameworks. The POMs in **1** and **2** support the metal–organic complexes via hydrogen bond interactions [17], while $[BW_{12}O_{40}]^{5-}$ in **3** coordinates with copper–organic complexes by Cu−O bonding, forming a one-dimensional (1-D) chain. With the change of POM species, the architectures of the POM-based Cu–organic complexes differ [18].

2. Experimental

2.1. *Materials and methods*

All reagents were purchased commercially and used without purification. $K_5[BW_{12}O_{40}]\cdot 15H_2O$ was prepared according to the literature [19]. Infrared spectra were recorded employing KBr pellets from 4000 to 400 cm^{-1}. Element analyses (C, N, and H) were carried out using a Perkin-Elmer 2400. Thermogravimetric analysis (TGA) data were collected on DTG-60AH under N_2 with 30 mL min^{-1} gas flow. Powder X-ray diffraction (PXRD) data were obtained on a Siemens D5005 diffractometer. UV–vis spectra were obtained from a Lab Tech UV-Power diode-array spectrometer. Fluorescence spectra were measured on an F-4600 FL spectrophotometer. EPR spectra were recorded from a Bruker EMX-220 digital X-Band (υ = 9.43 GHz) spectrophotometer. Electrochemical measurements were performed with a CHI660b electrochemical workstation. A traditional three-electrode system was used. A saturated calomel electrode was used as a reference electrode, and the counter electrode was a Pt wire. Bulk-modified carbon paste electrodes (CPEs) of **1–3** were used as the working electrodes. The CPEs were prepared according to the literature [35].

2.2. *Synthesis of $[Cu^{II}_2(phen)_2(4,4'\text{-bipy})(H4,4'\text{-bipy})_2(H_2O)_2][PMo_{12}O_{40}]_2{\cdot}2H_2O$ (1)*

A mixture of $H_3[PMo_{12}O_{40}]{\cdot}13H_2O$ (0.183 g, 0.1 mM), phen (0.02 g, 0.1 mM), 4,4′-bipy (0.019 g, 0.1 mM), and $Cu(NO_3)_2{\cdot}3H_2O$ (0.025 g, 0.1 mM) was dissolved in 10 mL distilled water. Then, it was stirred for 30 min, and the pH of the mixture was adjusted to 4.0 using 1 M NaOH. The suspension was transferred into a 25 mL Teflon-lined stainless steel container and kept at autogenous pressure at 160 °C for 3 days. After slowly cooling to room temperature, green block crystals of **1** were obtained with yield of 71% (based on Mo). Anal. Calcd for $C_{54}H_{50}Cu_2Mo_{24}N_{10}O_{84}$: C, 13.87; H, 1.08; N, 2.99%. Found: C, 13.78; H, 1.168; N, 3.01%. IR (KBr pellet, cm^{-1}): 720 (s), 800 (s), 874 (s), 957 (s), 1059 (s), 1107 (w), 1146 (m), 1210 (w), 1223 (w), 1248 (w), 1309 (w), 1322 (w), 1344 (w), 1399 (w), 1421 (s), 1492 (m).

2.3. *Synthesis of $[Cu^{II}(phen)_2(H4,4'\text{-bipy})][PW_{12}O_{40}]{\cdot}H_2O$ (2)*

A mixture of $H_3[PW_{12}O_{40}]$ (0.288 g, 0.1 mM), $Cu(NO_3)_2{\cdot}3H_2O$ (0.024 g, 0.1 mM), phen (0.02 g, 0.1 mM), and 4,4′-bipy (0.019 g, 0.1 mM) was dissolved in 10 mL of distilled water with stirring at room temperature. The pH of the mixture was adjusted to 5.0 with 1 M NaOH. Then, the mixture was transferred into a 25 mL Teflon-lined stainless steel container and kept at 160 °C for 3 days. After gradually cooling to room temperature, blue block crystals of **2** were obtained in 58% yield (based on W). Anal. Calcd for $C_{34}H_{27}N_6O_{41}PW_{12}Cu$: C, 11.74; H, 0.78; N, 2.42%. Found: C, 11.80; H, 0.82; N, 2.50%. IR (KBr pellet, cm^{-1}): 720 (s), 765 (w), 813 (s), 893 (s), 976 (s), 1075 (s), 1104 (m), 1146 (s), 1207 (w), 1223.13 (w), 1258 (w), 1306 (w), 1319 (w), 1344 (w), 1370 (w), 1431 (m), 1492.17 (m), 1521 (m), 1562 (w), 1585 (w), 1610 (w), 1626 (w), 1642 (w).

2.4. *Synthesis of $[Cu^{II}_2(phen)_2(4,4'\text{-bipy})(BW_{12}O_{40})(H_2O)_2](H_24,4'\text{-bipy})_{0.5}{\cdot}3H_2O$ (3)*

A mixture of $K_5[BW_{12}O_{40}]{\cdot}15H_2O$ (0.332 g, 0.1 mM), $Cu(CH_3COO)_2{\cdot}H_2O$ (0.032 g, 0.2 mM), phen (0.02 g, 0.1 mM), and 4,4′-bipy (0.019 g, 0.1 mM) was dissolved in 10 mL of distilled water with stirring for 30 min. The pH of the mixture was adjusted to 3.5 using 1 M NaOH. Then, the mixture was transferred into a 25 mL Teflon-lined stainless steel container and kept at 160 °C for 4 days. After gradually cooling to room temperature, blue block crystals of **3** were obtained with yield of 55% (based on W). Anal. Calcd for $C_{39}H_{39}N_7O_{45}BW_{12}Cu_2$: C, 12.77; H, 1.07; N, 2.67%. Found: C, 12.86; H, 0.86; N, 2.69%. IR (KBr pellet, cm^{-1}): 717 (m), 819 (s), 899 (s), 954 (s), 998 (s), 1072 (m), 1111 (w), 1149 (m), 1200 (w), 1216 (w), 1325 (w), 1341 (w), 1415 (s), 1488 (m), 1521 (m), 1585.05 (w), 1617 (s).

2.5. *X-ray crystallography*

Single-crystal data for **1–3** were collected at 298 K on a Bruker SMART CCD diffractometer with graphite-monochromated MoK_α radiation ($\lambda = 0.71073$ Å). The structures were refined by full-matrix least-squares on F^2 using SHELXL 97 [20], and all non-hydrogen atoms were refined anisotropically. Anisotropic thermal parameters were refined for crystals of **1–3**. A summary of crystal data and structure refinement for **1–3** is listed in table 1. Table 2 shows selected bond lengths and angles for **1–3**. All hydrogen bond distances (Å) and angles (°) of **1–3** are listed in table 3.

Table 1. Crystal data and structure refinements for **1–3**.

	1	**2**	**3**
Formula	$C_{54}H_{50}N_{10}O_{84}P_2Mo_{24}Cu_2$	$C_{34}H_{27}N_6O_{41}PW_{12}Cu$	$C_{39}H_{39}N_7O_{45}BW_{12}Cu_2$
Mr	4674.64	3476.22	3669.76
T (K)	298(2)	298(2)	298(2)
Crystal system	Triclinic	Orthorhombic	Triclinic
Space group	$P\bar{1}$	$P2(1)2(1)2(1)$	$P\bar{1}$
a (Å)	10.6022(8)	10.96(2)	12.6857(7)
b (Å)	11.7176(9)	23.19(4)	15.0965(8)
c (Å)	22.116(2)	23.67(5)	17.1388(9)
α (°)	77.616(1)	90	86.776(4)
β (°)	83.247(2)	90	87.817(4)
γ (°)	82.511(2)	90	86.569(4)
V (Å$^{3)}$	2649.3(4)	6016(20)	3269.2(3)
Z	1	4	2
μ (mm^{-1})	3.275	23.314	21.757
$F(0\ 0\ 0)$	2212	6132	3266
Reflns.	13,183	25,758	25,758
R_{int}	0.0274	0.0897	0.0739
Data/restraints/parameters	9121/0/832	10518/0/893	11507/0/994
GOF	1.041	1.000	1.077
$R_1[I > 2\sigma(I)]$[a]	0.0453	0.0582	0.0685
wR_2 (all data)[b]	0.1229	0.1334	0.1313
$\Delta\rho_{max,min}$ (e Å^{-3})	1.168 and −1.404	3.746 and −3.361	2.784 and −2.528

[a]$R_1 = \sum||F_o| - |F_c||/\sum|F_o|$.
[b]$wR_2 = \sum[w(F_o^2 - F_o^2)^2]/\sum[w(F_o^2)^2]^{1/2}$.

3. Results and discussion

3.1. *Syntheses*

The assembly of inorganic–organic hybrid materials based on POMs under hydrothermal conditions is an effective method to produce new compounds [21, 29]. In the synthesis, **1–3** were obtained at pH values of 4.0, 5.0, and 3.5, respectively. In the weak acidic media, the Keggin-type anions were stable and have higher negative charges, which were easy to combine with the transition metal complexes. When the pH value was lower or higher than the optimal value, **1–3** cannot be obtained; thus, pH plays an important role in the crystallization of **1–3**. Additionally, the nature of the metal salt is also crucial for the formation of **1–3**. If $Cu(NO_3)_2{\cdot}3H_2O$ was replaced by $CuCl_2{\cdot}2H_2O$ as the starting material for **1** and **2**, only amorphous powder was obtained. When $Cu(CH_3COO)_2{\cdot}H_2O$ was replaced with $Cu(NO_3)_2{\cdot}3H_2O$ or $CuCl_2{\cdot}2H_2O$ in **3**, no suitable crystals for single-crystal X-ray diffraction were obtained. The kind of POM also influenced the framework of the hybrids. Different from other reported compounds, compounds **1–3** show the effect of pH value and the type of POM on the inorganic–organic hybrid compounds.

3.1.1. Structure description of 1. X-ray diffraction analysis reveals that **1** exists in triclinic space group $P\bar{1}$. The asymmetric unit of **1** contains two Keggin $[PMo_{12}O_{40}]^{3-}$ (abbreviated as PMo_{12}) anions, a $[Cu^{II}_2(phen)_2(4,4'\text{-bipy})(H4,4'\text{-bipy})_2(H_2O)_2]^{3+}$ moiety, and two lattice waters (figure 1). In $[Cu^{II}_2(phen)_2(4,4'\text{-bipy})(H4,4'\text{-bipy})_2(H_2O)_2]^{3+}$, Cu(1) has a square pyramidal geometry, defined by one water, four nitrogens from one phen and two 4,4′-bipy ligands [figure S1(a), see online supplemental material at http://dx.doi.org/10.1080/00958972.2015.1009906]. The bond lengths of Cu(1)−N are 1.977(9)–2.039(8) Å and that

Table 2. Selected bond lengths and angles for **1–3**.

Compound **1**	
Cu(1)–N(3)	1.989(9)
Cu(1)–N(5)	2.030(8)
Cu(1)–N(1)	2.039(8)
Cu(1)–O(45)	2.294(8)
N(2)–Cu(1)–N(3)	161.7(3)
N(2)–Cu(1)–N(5)	97.5(3)
N(3)–Cu(1)–N(5)	89.0(4)
N(2)–Cu(1)–N(1)	82.6(4)
N(3)–Cu(1)–N(1)	90.7(4)
N(5)–Cu(1)–N(1)	179.4(3)
N(2)–Cu(1)–O(45)	98.3(4)
N(3)–Cu(1)–O(45)	98.4(4)
N(5)–Cu(1)–O(45)	92.6(3)
N(1)–Cu(1)–O(45)	88.0(3)
Symmetry codes for **1**: #1 $-x + 2, -y, -z + 1$; #2 $-x + 1, -y + 2, -z$; #3 $-x, -y + 1, -z$.	
Compound **2**	
N(3)–Cu(1)	2.020(4)
N(4)–Cu(1)	2.100(4)
N(5)–Cu(1)	2.028(10)
N(6)–Cu(1)	1.990(3)
N(6)–Cu(1)–N(3)	178.0(14)
N(6)–Cu(1)–N(4)	98.7(15)
N(3)–Cu(1)–N(4)	80.5(16)
N(6)–Cu(1)–N(1)	90.8(13)
N(3)–Cu(1)–N(1)	88.2(14)
N(4)–Cu(1)–N(1)	124.0(12)
N(6)–Cu(1)–N(5)	79.3(14)
N(3)–Cu(1)–N(5)	102.7(15)
N(4)–Cu(1)–N(5)	121.5(12)
N(1)–Cu(1)–N(5)	114.4(13)
Symmetry transformations used to generate equivalent atoms.	
Compound **3**	
Cu(1)–N(1)	1.984(19)
Cu(1)–N(3)	1.990(2)
Cu(1)–N(4)	1.997(19)
Cu(1)–O(14)	2.198(16)
Cu(2)–N(5)	1.960(2)
Cu(2)–N(6)	1.960(2)
Cu(2)–O(45)	1.990(18)
Cu(2)–N(2)	1.990(2)
Cu(2)–O(46)	2.382(17)
O(34)–Cu(1)–N(1)	88.3(8)
O(34)–Cu(1)–N(3)	170.6(7)
N(1)–Cu(1)–N(3)	95.9(9)
O(34)–Cu(1)–N(4)	91.4(7)
N(1)–Cu(1)–N(4)	165.5(9)
N(3)–Cu(1)–N(4)	82.5(8)
O(34)–Cu(1)–O(14)	98.1(6)
N(1)–Cu(1)–O(14)	99.2(8)
N(3)–Cu(1)–O(14)	89.6(7)
N(4)–Cu(1)–O(14)	95.2(7)
N(5)–Cu(2)–N(6)	84.0(9)
N(5)–Cu(2)–O(45)	90.5(8)
N(6)–Cu(2)–O(45)	173.5(8)

(*Continued*)

Table 2. *(Continued)*.

N(5)–Cu(2)–N(2)	177.2(9)
N(6)–Cu(2)–N(2)	95.1(9)
O(45)–Cu(2)–N(2)	90.6(9)
N(5)–Cu(2)–O(46)	86.9(7)
N(6)–Cu(2)–O(46)	88.9(8)
O(45)–Cu(2)–O(46)	87.5(7)
N(2)–Cu(2)–O(46)	95.7(8)

Symmetry codes for **3**: #1 $-x+2, -y+1, -z+1$; #2 $-x+1, -y+2, -z$; #3 $-x+2, -y+2, -z+1$.

Table 3. Hydrogen-bonding geometries (Å, °) of **1–3**.

	D–H···A	d(D–H)	d(H···A)	d(D···A)	∠(D–H···A)
Compound **1**	N(4)–H(4)···O(11)	0.86	2.20	3.0462	166
	O(45)–H(45C)···O(5)	0.85	2.03	2.8822	178
	O(45)–H(45D)···O(46)	0.85	2.13	2.9829	178
	O(46)–H(46C)···O(21)	0.85	2.18	3.0245	177
	O(46)–H(46D)···O(39)	0.85	2.32	3.1647	177
Compound **2**	N(2)–H(2)···O(41)	0.86	1.81	2.6476	165
	O(41)–H(41C)···O(13)	0.85	2.06	2.9094	175
	O(41)–H(41D)···O(29)	0.85	2.18	3.0299	175
	C(23)–H(23)···O(32)	0.93	2.57	3.1042	117
	C(2)–H(2A)···O(17)	0.93	2.50	3.1434	127
Compound **3**	N(7)–H(7)···O(48)	0.86	1.88	2.734	167
	O(45)–H(45B)···O(36)	0.85	2.60	3.113	120
	O(45)–H(45B)···O(37)	0.85	2.00	2.792	155
	O(45)–H(45C)···O(49)	0.85	1.79	2.593	156
	O(46)–H(46A)···O(22)	0.85	2.06	2.903	173
	O(46)–H(46B)···O(46)	0.85	2.32	3.173	174
	O(47)–H(47C)···O(19)	0.85	2.22	3.063	171
	O(47)–H(47D)···O(40)	0.85	2.10	2.943	171
	O(48)–H(48C)···O(30)	0.85	2.40	3.243	165
	O(48)–H(48D)···O(42)	0.85	2.13	2.963	165
	O(49)–H(49C)···O(47)	0.85	1.90	2.753	177
	O(49)–H(49D)···O(35)	0.85	2.23	3.083	176

of Cu(1)−O_{auqa} is 2.294(8) Å. The bidentate-chelating phen bonds with Cu(1) [figure S1(b)]. Three 4,4′-bipy ligands coordinated with two Cu(1) ions are classified into two types [figure S1(c)]. One 4,4′-bipy is a bidentate bridge linking two Cu–phen units together. Two monoprotonated 4,4′-bipy are monodentate ligands, important for formation of hydrogen bonds. PMo_{12} as an inversion center interacts with fragments through hydrogen bonds. Furthermore, each PMo_{12} unit is surrounded by two $[Cu^{II}_2(phen)_2(4,4'\text{-bipy})(H4,4'\text{-bipy})_2(H_2O)_2]^{3+}$ moieties to generate a 2-D supramolecular network (figure 2). There are two kinds of hydrogen bonds in **1**. One is between nitrogens from monoprotonated 4,4′-bipy and oxygen of $[PMo_{12}O_{40}]^{3-}$ with bond lengths N(4)–H(4)···O(11) of 3.0462 Å; the others exist between oxygen from $[PMo_{12}O_{40}]^{3-}$ and lattice water molecules [O(46)–H(46C)···O(21): 3.0245 Å, O(46)–H(46D)···O(39): 3.1647 Å], and lattice water molecules and coordinated water molecules with the bond length O(45)–H(45D)···O(46) of 2.9829 Å, and $[PMo_{12}O_{40}]^{3-}$ polyoxoanion with coordinated waters [O(45)–H(45C)···O(5) 2.8822 Å].

3.1.2. Structure description of 2. Compound **2** crystallizes in orthorhombic *P*2(1)2(1)2(1) space group. It is constructed from a Keggin-type $[PW_{12}O_{40}]^{3-}$ (abbreviated as PW_{12})

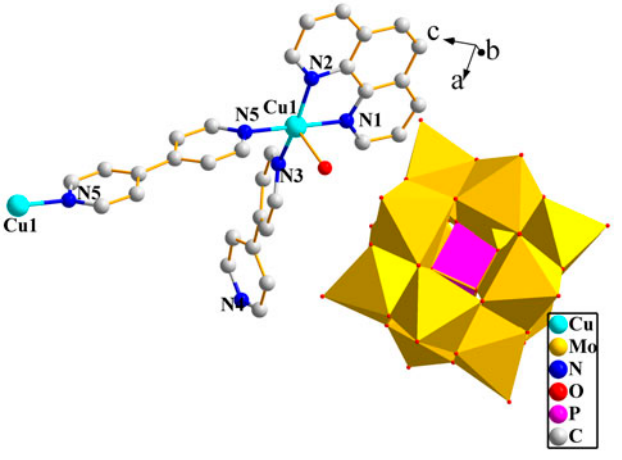

Figure 1. A polyhedral view of **1**; because the two copper ions have the same coordination environment, only one copper is shown. The water and hydrogens are omitted for clarity. Brown octahedra for $\{MoO_6\}$, crimson tetrahedra for $\{PO_4\}$. C, gray; N, dark blue; O, red; Cu, cyan (see http://dx.doi.org/10.1080/00958972.2015.1009906 for color version).

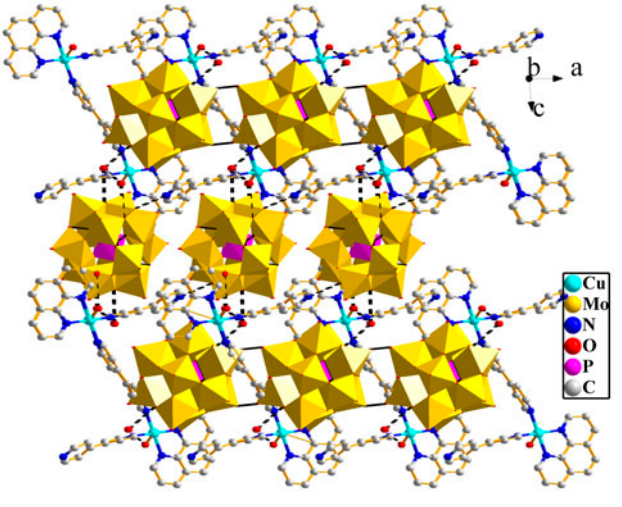

Figure 2. 2-D supramolecular framework of **1** viewed along the *b* axis from hydrogen bonding, showing the PMo_{12} was incorporated into the framework of $[Cu^{II}_2(phen)_2(4,4'\text{-bipy})(H4,4'bipy)_2(H_2O)_2]$, producing a 2-D structure. The dotted lines represent hydrogen bonds.

anion, one $[Cu^{II}(phen)_2(H4,4'\text{-bipy})]$, and a water molecule (figure 3). In $[Cu^{II}(phen)_2(H4,4'\text{-bipy})]$, Cu(1) with a trigonal bipyramid configuration is coordinated with five nitrogens from two phen ligands and a protonated 4,4′-bipy [figure S2(a)]. The bond lengths are 1.990(3)–2.100(4) Å for Cu(1)–N. The coordination modes of phen are identical to that in **1** [figure S2(b)]. Monodentate 4,4′-bipy is monoprotonated, bonding with copper ion [figure S2(c)]. Free $[PW_{12}O_{40}]^{3-}$ cluster anion links Cu–organic complexes via hydrogen bonds, leading to a 1-D chain arrangement. Furthermore, PW_{12} clusters with nearby

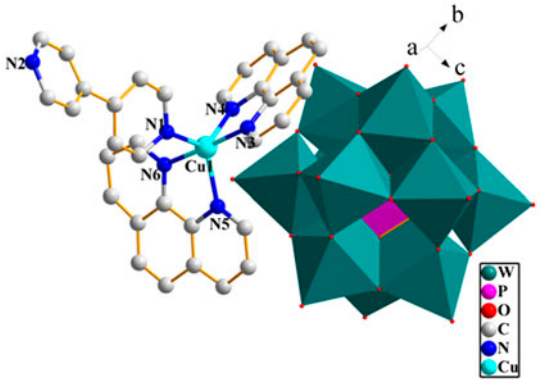

Figure 3. A polyhedral view of **2**. The water molecule and hydrogens are omitted for clarity. Blue octahedra for $\{WO_6\}$, crimson tetrahedra for $\{PO_4\}$. C, gray; N, dark blue; O, red; Cu, cyan (see http://dx.doi.org/10.1080/00958972.2015.1009906 for color version).

transition metal complexes are aggregated by weak C···O interactions, which give a 2-D supramolecular framework (figure 4). Therefore, each PW_{12} unit could be decorated by three Cu–organic segments. The typical hydrogen bonds are N(2)–H(2)···O(41) 2.6476 Å, which are offered by protonated 4,4′-bipy ligands and lattice waters. Additionally, the distance of O(41)–H(41C)···O(13) is 2.9094 Å and that of O(41)–H(41D)···O(29) is 3.0299 Å, between PW_{12} anion and water molecules. The C···O bonds are C(2)–H(2A)···O(17) with the bond length of 3.1434 and 3.1042 Å for C(23)–H(23)···O(32).

3.1.3. Structure description of 3. **3** crystallizes in triclinic system with space group $P\bar{1}$ and consists of an anion $[Cu^{II}_2(phen)_2(4,4'\text{-bipy})(BW_{12}O_{40})(H_2O)_2]$, three lattice water molecules, and half a protonated 4,4′-bipy as an inversion ion. In $[Cu^{II}_2(phen)_2(4,4'\text{-bipy})(BW_{12}O_{40})(H_2O)_2]$, there are two crystallographically independent Cu^{II} ions (Cu(1) and Cu(2)) (figure 5). Cu1 is five coordinate defined by three N from phen and 4,4′-bipy ligands and two terminal oxygens from two $[BW_{12}O_{40}]^{5-}$ cluster anions (abbreviated to BW_{12}), showing a square bipyramid spatial configuration. Cu2 with square bipyramid geometry is five coordinate with three N from one phen and one 4,4′-bipy and two coordinated waters [figure S3(a) and (b)]. The bond lengths around Cu(1) and Cu(2) are 1.984(19)–1.977(19) Å for Cu(1)–N, 1.960(2)–1.990(2) Å for Cu(2)–N, 1.964(16)–2.198(16) Å for Cu(1)−O, and 1.990(18)–2.382(17) Å for Cu(2)−O_{auqa}. Phen is bidentate [figure S3(c)], and 4,4′-bipy is a bidentate bridge connecting the two Cu-phen fragments [figure S3(d)]; the discrete $H_2$4,4′-bipy ion is not coordinated. BW_{12} in **3** combines with adjacent copper–organic fragments by Cu(1)–O bonding yielding a 1-D chain-like structure; the 1-D chains are further packed into the 2-D supramolecular network through hydrogen bond interactions (figure 6). The hydrogen bonds reside between discrete protonated 4,4′-bipy ligands and lattice waters [N(7)–H(7)···O(48) 2.734 Å], BW_{12} anions and lattice water molecules [O(47)–H(47C)···O(19) 3.063 Å, O(47)–H(47D)···O(40) 2.943 Å, O(48)–H(48C)···O(30) 3.243 Å, O(48)–H(48D)···O(42) 2.963 Å, O(49)–H(49D)···O(35) 3.083 Å], coordinated water molecules and BW_{12} polyoxoanions [O(45)–H(45B)···O(36) 3.113 Å, O(45)–H(45B)···O(37) 2.792 Å, O(46)–H(46A)···O(22) 2.903 Å] and between lattice water molecules and coordinated water molecules with O(45)–H(45C)···O(49) distance of 2.593 Å.

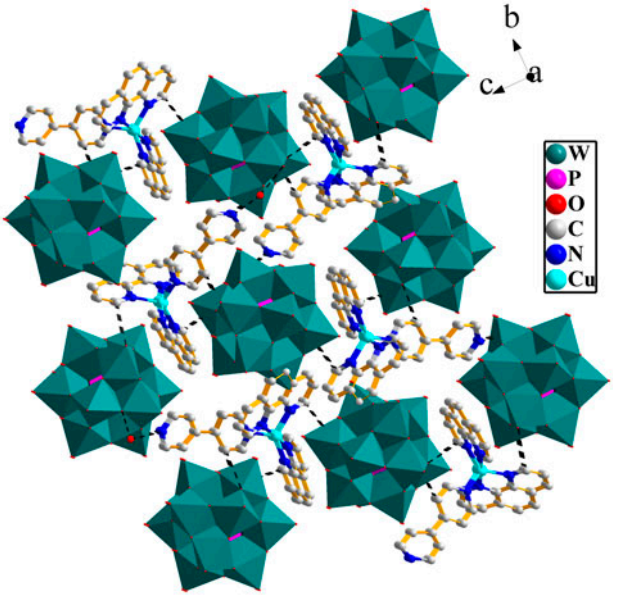

Figure 4. A 2-D supramolecular network of **2** viewed along the *a* axis generated via hydrogen-bonding interactions and weak C–H···O bonding. The dotted lines represent hydrogen bonds.

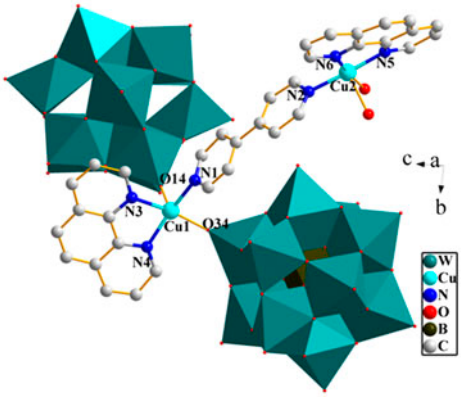

Figure 5. A view of the 1-D chain in **3**. Water molecules and hydrogens are omitted for clarity. Blue octahedra for $\{WO_6\}$, adobe tetrahedra for $\{PO_4\}$. C, gray; N, dark blue; O, red; Cu, cyan (see http://dx.doi.org/10.1080/00958972.2015.1009906 for color version).

Compounds **1–3** are inorganic–organic hybrids based on different Keggin-type POMs, and they present distinct structural features. Compounds **1** and **2** are 2-D networks packing from mononuclear fragments with POMs anions. Compound **3** is a 2-D layer framework, due to the connectivity of 1-D chain with neighboring moieties via hydrogen bond interactions. In the assembly process, the pH and POM play important roles in the inorganic–organic hybrid materials. In **1** and **2**, PMo_{12} and PW_{12} anions do not coordinate with copper ions, but in **3** BW_{12} units are linked with $[Cu^{II}_2(phen)_2(4,4'\text{-bipy})(H_2O)]$,

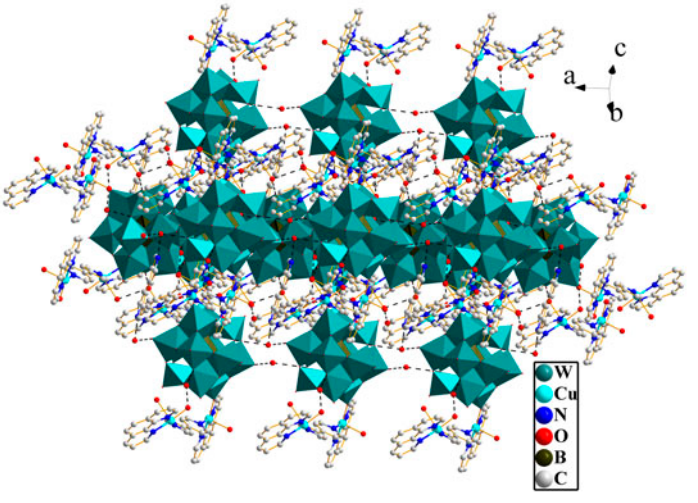

Figure 6. 2-D supramolecular framework of **3** viewed along the [2 2 1] plane from hydrogen bond interactions. The dotted lines represent hydrogen bonds.

resulting in a 1-D chain-like construction. Though PMo_{12}, PW_{12}, and BW_{12} are all Keggin-type POMs, they exhibit different coordination abilities and electron densities under different pH conditions. Therefore, the types of POMs and pH have effects on the formation of various frameworks (scheme 1).

3.2. *XRD and FT-IR spectra*

The powder XRD patterns of **1–3** and their corresponding simulated peaks show good coincidence (figure S4), which confirms their purity. IR spectra of **1–3** are listed in figure S5. The characteristic peaks at 720, 800, 877, 959, and 1064 cm^{-1} for **1** are ascribed to ν(Mo–O_c–Mo), ν(Mo–O_b–Mo), ν(Mo–O_d), and ν(P–O_a) of $[PMo_{12}O_{40}]^{3-}$ [22]. The characteristic bands at 813,

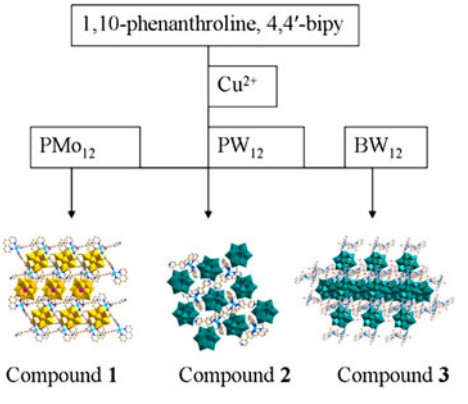

Scheme 1. Schematic views of three hybrids based on Keggin-type POMs.

893, 976, and 1075 cm^{-1} for **2** are attributed to ν(W–O_c–W), ν(W–O_b–W), ν(W–O_d), and ν(P–O_a) of $[PW_{12}O_{40}]^{3-}$ [30]. The characteristic peaks at 819, 899, 954, and 998 cm^{-1} for **3** correspond to ν(W–O_c–W), ν(B–O_a), and ν(W–O_d) of $[BW_{12}O_{40}]^{5-}$. The characteristic peaks at 1146–1627 cm^{-1} for **1–3** are assigned to phen and 4,4′-bipy [23].

3.3. *TGA studies*

Thermogravimetric analyses were tested of **1**, **2**, and **3** on the DTG-60AH from 30 to 800 °C under N_2 with gas flow of 30 mL min^{-1}. The corresponding curves of **1–3** are listed in figure S6. For **1**, the loss of weight from 30 to 300 °C is 1.69% (Calcd 1.49%), corresponding to loss of water. Weight loss of 19.01% (Calcd 17.73%) between 300 and 460 °C is ascribed to the release of phen and 4,4′-bipy. For **2**, the loss of weight from 30 to 570 °C is 4.54% (Calcd 5.03%) and corresponds to the removal of lattice water and protonated 4,4′-bipy. For **3**, the weight loss from 30 to 235 °C is 4.84% (Calcd 4.6%) and is attributed to the removal of coordinated water, lattice water molecules, and dehydration of protonated 4,4′-bipy molecules. The weight loss from 235 to 670 °C is 16% (Calcd 14.07%), which corresponds to decomposition of phen and 4,4′-bipy and partial degradation of BW_{12}.

3.4. *Photoluminescent properties*

Phen possesses fluorescence properties [25]. The fluorescence spectra of **1–3** were measured on an F-4600 FL spectrophotometer. The emission spectra of **1–3** are shown in figure S7. The results show that the emission peaks of 4,4'-bipy are located at 437 nm upon excitation at 359 nm. The emission peaks of phen are at 370 and 383 nm with excitation at 280 nm. However, the emission peaks of **1**, **2**, and **3** are redshifted to 502, 476 and 472 nm, respectively. The reason for redshift in **1–3** may be that the combination of phen and 4,4′-bipy with copper ions increases the rigidity of ligands, while decreasing the energy of excited states. The results suggest a strong interaction of phen, 4,4′-bipy, and POMs in **1–3**, which is critical for formation of the 2-D structure.

3.5. *UV–vis spectra*

The solid-state UV–vis spectra of **1–3** were measured in $BaSO_4$ matrices from 200 to 800 nm. The UV–vis spectra of **1** [figure S8(a)] exhibit two obvious absorptions at 273 and 355 nm, which are ascribed to the ligand-to-metal charge transfer of O → Mo. The UV–vis spectra of **2** [figure S8(b)] display two intense absorptions at 255 and 306 nm, which are assigned to the ligand-to-metal charge transfer of O → W [24]. The UV–vis spectra of **3** [figure S8(c)] show two strong absorptions at 255 and 296 nm, which are attributed to ligand-to-metal charge transfer of O → W.

3.6. *EPR spectra*

EPR spectra for **1**, **2**, and **3** are shown in figure 7. Compounds **1** and **3** show broad signals centered at $g = 2.071$ and 2.107, respectively. The signals in **1** and **3** indicate the presence of Cu^{II} ions with square pyramidal stereochemistry and the unpaired electron in the $d_{x^2-y^2}$ orbital [33]. Compound **2** exhibits an intense signal at $g = 2.084$, which is attributed to Cu^{II}

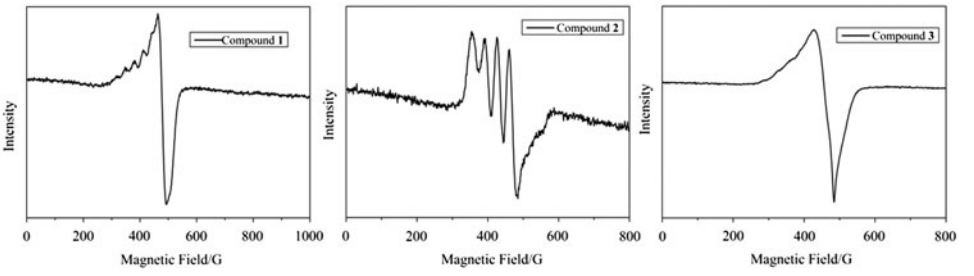

Figure 7. X-band EPR spectra of **1–3** recorded at room temperature.

ions having trigonal bipyramidal environment with unpaired electron in the $d_{x^2-y^2}$ orbital. The other three signals at about 425G, 390G, and 355G are assigned to a small amount of exchanged Cu^{II} species [34].

3.7. *Electrochemistry*

Over the past several years, considerable interest has been focused on electrochemical studies of POM-based hybrids [26–28]. Cyclic voltammetry experiments were performed to examine the redox properties of **1–3** in 1 M H_2SO_4 solution. Because **1**, **2**, and **3** have low solubility in water and organic solvents, the bulk-modified CPEs become the best way to investigate the electrochemical properties of **1–3**. The cyclic voltammograms for **1**-CPE, **2**-CPE, and **3**-CPE in 1 M H_2SO_4 are presented in figure 8. From −0.300 to 1.100 V for **1**–CPE, there exist three pairs of reversible redox peaks (I–I′, II−II′, and III−III′). The peak potentials $E_{1/2} = (E_{pc} + E_{pa})/2$ of the three pairs of redox peaks are +0.298, +0.147, and −0.085 V, respectively. The redox peaks of I–I′, II−II′, and III−III′ are attributed to three consecutive two-electron processes of Mo. In the range of −0.750 to 0.600 V for **2**-CPE, there are two pairs of reversible redox peaks (I–I′, II−II′), and the corresponding $E_{1/2}$ values are −0.410 and −0.598 V, respectively, which are ascribed to two consecutive two-electron processes of W. In the potential range of −0.640 to 1.000 V for **3**–CPE, two pairs of reversible redox peaks (I–I′, II−II′) appear, and their $E_{1/2}$ values are +0.144 and −0.343 V, respectively. They are assigned to two consecutive two-electron processes of W, respectively.

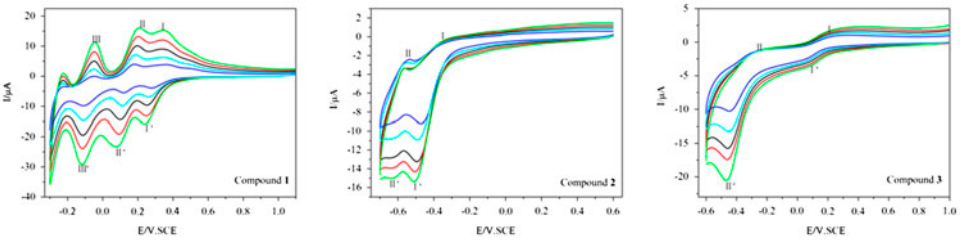

Figure 8. Cyclic voltammograms at different scan rates for **1-**, **2-**, and **3**-CPE in 1 M H_2SO_4 solution. From inner to outer: 50, 75, 100, 125, and 150 mV s^{-1}.

4. Conclusion

Three inorganic–organic hybrid compounds based on Keggin-type POMs have been prepared. In those three compounds, copper ions present different linking modes and 4,4′-bipy ligands have multiple coordination types. Compared with the reported hybrid complexes based on POMs and copper ions [31, 32, 37], the three POM-based compounds contain both phen and 4,4′-bipy ligands and have different conformations. The synthesis of **1**–**3** supplies a simple approach for the construction of new POM-based hybrid materials. Though PMo_{12}, PW_{12}, and BW_{12} anions are all Keggin types, they have different coordination abilities. In **1** and **2**, PMo_{12} and PW_{12} units are discrete anions, and in **3**, BW_{12} is monodentate to connect with copper ion. In addition, protonated 4,4′-bipy ligands are coordinated with copper ions in **1** and **2**, while in **3** the protonated 4,4′-bipy serves as an inversion ion to balance the negative charges. Because PMo_{12}, PW_{12}, and BW_{12} heteropolyanions possess diverse electron densities under different pH values, they show distinct coordination abilities to metal complexes. The structural analysis reveals that their differences influence the configurations of the hybrid compounds. Therefore, POMs cluster and pH play significant roles in formation of diverse POM-based inorganic–organic hybrid compounds in the Cu/phen/4,4′-bipy system.

Supplementary material

Crystallographic Data Center with CCDC reference number 1014491 for **1**, 1014492 for **2**, and 1014493 for **3** have data that can be obtained free of charge from the Cambridge Crystallographic Data Center via www.ccdc.cam.ac.uk/data_request/cif. Some additional structural figures for **1**, **2**, and **3** and physical characterizations including IR, PXRD, TG curves, fluorescence spectra, and UV–vis spectra.

Funding

This work was financially supported by the National Natural Science Foundation [grant number 20971014], [grant number 21271024]; the 111 Project (B07012) in China and Beijing Natural Science Foundation [grant number 2112037].

References

[1] A.M. Khenkin, I. Efremenko, J.M.L. Martin, R. Neumann. *J. Am. Chem. Soc.*, **135**, 19304 (2013).
[2] H.S. Xu, L.L. Li, B. Liu, G.L. Xue, H.M. Hu, F. Fu, J.W. Wang. *Inorg. Chem.*, **48**, 10275 (2009).
[3] Z.X. Zhang, M. Sadakane, T. Murayama, S. Izumi, N. Yasuda, N. Sakaguchi, W. Ueda. *Inorg. Chem.*, **53**, 903 (2014).
[4] Y. Zhang, J.Q. Shen, L.H. Zheng, Z.M. Zhang, Y.X. Li, E.B. Wang. *Cryst. Growth Des.*, **14**, 110 (2014).
[5] Y.C. Ji, T.F. Li, Y.F. Song. *Ind. Eng. Chem. Res.*, **53**, 11566 (2014).
[6] (a) B. Matt, C. Coudret, C. Viala, D. Jouvenot, F. Loiseau, G. Izzet, A. Proust. *Inorg. Chem.*, **50**, 7761 (2011); (b) B. Qin, H.Y. Chen, H. Liang, L. Fu, X.F. Liu, X.H. Qiu, S.Q. Liu, R. Song, Z.Y. Tang. *J. Am. Chem. Soc.*, **132**, 2886 (2010).
[7] Z. Han, Y. Zhao, J. Peng, Y. Feng, J. Yin, Q. Liu. *Electroanalysis*, **17**, 1097 (2005).
[8] X. Wang, M.M. Zhang, X.L. Hao, Y.H. Wang, Y. Wei, F.S. Liang, L.J. Xu, Y.G. Li. *Cryst. Growth Des.*, **13**, 3454 (2013).
[9] R. Kawahara, S. Uchida, N. Mizuno. *Inorg. Chem.*, **53**, 3655 (2014).
[10] P. Mialane, A. Dolbecq, J. Marrot, E. Rivière, F. Sécheresse. *Chem. Eur. J.*, **11**, 1771 (2005).

[11] (a) E. Coronado, C. Giménez-Saiz, C.J. Gómez-García, S.C. Capelli. *Angew. Chem.*, **116**, 3084 (2004); *Angew. Chem. Int. Ed.*, **43**, 3022 (2004); (b) Y. Ishii, Y. Takenaka, K. Konishi. *Angew. Chem.*, **116**, 2756 (2004); *Angew. Chem. Int. Ed.*, **43**, 2702 (2004).
[12] Z.K. Qu, K. Yu, Z.F. Zhao, Z.H. Su, J.Q. Sha, C.M. Wang, B.B. Zhou. *Dalton Trans.*, **43**, 6744 (2014).
[13] C.Y. Sun, Y.G. Li, E.B. Wang, D.R. Xiao, H.Y. An, L. Xu. *Inorg. Chem.*, **46**, 1563 (2007).
[14] Q.X. Han, X.P. Sun, J. Li, P.T. Ma, J.Y. Niu. *Inorg. Chem.*, **53**, 2006 (2014).
[15] L.M. Wang, Y. Fan, Y. Wang, L.N. Xiao, Y.Y. Hu, Y. Peng, T.G. Wang, Z.M. Gao, D.F. Zheng, X.B. Cui, J.Q. Xu. *J. Solid State Chem.*, **191**, 257 (2012).
[16] L.M. Wang, Y. Wang, Y. Fan, L.N. Xiao, Y.Y. Hu, Z.M. Gao, D.F. Zheng, X.B. Cui, J.Q. Xu. *CrystEngComm*, **16**, 430 (2013).
[17] X.L. Wang, J. Li, A.X. Tian, D. Zhao, G.C. Liu, H.Y. Lin. *Cryst. Growth Des.*, **11**, 3456 (2011).
[18] C.M. Liu, D.Q. Zhang, D.B. Zhu. *Cryst. Growth Des.*, **6**, 524 (2006).
[19] C.R. Deitcheff, M.R. Franck, R. Thouvenot. *Inorg. Chem.*, **22**, 207 (1983).
[20] G.M. Sheldrick. *SHELXL 97, Program for Crystal Structure Solution*, University of Göttingen, Göttingen (1997).
[21] W.H. Fang, L. Cheng, L. Huang, G.Y. Yang. *Inorg. Chem.*, **52**, 6 (2013).
[22] H.J. Guo, G.C. Yin. *J. Phys. Chem. C*, **115**, 17516 (2011).
[23] (a) L.K. Yu, Y. Yu, B.D. Jiang, B.B. Zhou. *CrystEngComm*, **15**, 5156 (2013); (b) H. Jin, Y.F. Qi, E.B. Wang, Y.G. Li, X.L. Wang, C. Qin, S. Chang. *Cryst. Growth Des.*, **6**, 2693 (2006).
[24] S. Himeno, M. Takamoto, T. Ueda. *J. Electroanal. Chem.*, **465**, 129 (1999).
[25] P.D. Fleischauer, P. Fleischauer. *Chem. Rev.*, **70**, 199 (1970).
[26] A. Proust, B. Matt, R. Villanneau, G. Guillemot, P. Gouzerh, G. Izzet. *Chem. Soc. Rev.*, **41**, 7605 (2012).
[27] M. Ibrahim, Y.X. Xiang, B.S. Bassil, Y.H. Lan, A.K. Powell, P.D. Oliveira, B. Keita, U. Kortz. *Inorg. Chem.*, **52**, 8399 (2013).
[28] (a) M. Sadakane, E. Steckhan. *Chem. Rev.*, **98**, 219 (1998); (b) Z.G. Jiang, K. Shi, Y.W. Lin, Q.M. Wang. *Chem. Commun.*, **50**, 2353 (2014); (c) Y. Zhang, J.Q. Shen, L.H. Zheng, Z.M. Zhang, Y.X. Li, E.B. Wang. *Cryst. Growth Des.*, **14**, 110 (2014).
[29] A.X. Tian, Y. Yang, N. Sun, J.C. Li, J. Ying, J.W. Zhang, X.L. Wang. *J. Coord. Chem.*, **67**, 1550 (2014).
[30] L.S. Felices, P. Vitoria, J.M. Gutiérrez-Zorrilla, L. Lezama, S. Reinoso. *Inorg. Chem.*, **45**, 7748 (2006).
[31] C.Y. Zhao, H.Y. Ma, H.J. Pang, S.B. Li, Y. Yu, T.T. Yu, Z.F. Zhang. *J. Coord. Chem.*, **67**, 2820 (2014).
[32] B.S. Zhang, C.S. Wu, J.P. Qiu, Y.X. Li, Z.X. Liu. *J. Coord. Chem.*, **67**, 785 (2014).
[33] J.P. Wang, S.Z. Li, Y. Shen, J.Y. Niu. *Cryst. Growth Des.*, **8**, 372 (2008).
[34] Y.H. Liu, P.T. Ma, J.P. Wang. *J. Coord. Chem.*, **61**, 936 (2008).
[35] J. Ying, M. Hou, X.J. Liu, A.X. Tian, X.L. Wang. *J. Coord. Chem.*, **65**, 218 (2012).
[36] (a) H. Jin, Y.F. Qi, E.B. Wang, Y.G. Li, X.L. Wang, C. Qin, S. Chang. *Cryst. Growth Des.*, **6**, 2693 (2006); (b) L. Yuan, C. Qin, X.L. Wang, E.B. Wang, S. Chang. *Eur. J. Inorg. Chem.*, **31**, 4936 (2008); (c) H. Jin, Y.F. Qi, E.B. Wang, Y.G. Li, C. Qin, X.L. Wang, S. Chang. *Eur. J. Inorg. Chem.*, **22**, 4541 (2006); (d) R. Lei, X.C. Chai, H.X. Mei, H.H. Zhang, Y.P. Chen, Y.Q. Sun. *J. Solid State Chem.*, **183**, 1510 (2010).
[37] (a) W.Q. Kan, J.M. Xu, Y.H. Kan, J. Guo, S.Z. Wen. *J. Coord. Chem.*, **67**, 195 (2014); (b) M.L. Qi, K. Yu, Z.H. Su, C.X. Wang, C.M. Wang, B.B. Zhou, C.C. Zhu. *J. Coord. Chem.*, **66**, 3531 (2013); (c) W.N. Li, F. Lin, X.X. Li, L.C. Zhang, W.S. You, Z.X. Jiang. *J. Coord. Chem.*, **66**, 2829 (2013); (d) M.L. Wei, L. Chen, X.Y. Duan. *J. Coord. Chem.*, **67**, 2809 (2014); (e) A.X. Tian, Y. Yang, N. Sun, J.C. Li, J. Ying, J.W. Zhang, X.L. Wang. *J. Coord. Chem.*, **67**, 1550 (2014); (f) L.M. Wang, H.Y. Guo, S. Li, Y.Y. Hu, Y. Wang, L.N. Xiao, D.C. Zhao, Z.M. Gao, D.F. Zheng, X.B. Cui, Y. Fan, J.Q. Xu. *J. Coord. Chem.*, **67**, 728 (2014); (g) X.L. Wang, Q. Gao, A.X. Tian, D. Zhao, X.J. Liu. *J. Coord. Chem.*, **66**, 358 (2013).